Supporting Information for

The Structural Basis for Homotropic and Heterotropic Cooperativity of Midazolam Metabolism by Human Cytochrome P450 3A4†

Arthur G. Roberts[a,e], *Jing Yang*[d], *James R. Halpert*[b], *Sidney D. Nelson*[c], *Kenneth T. Thummel*[d], *and William M. Atkins*[c]

[a]University of Georgia, Department of Pharmaceutical and Biomedical Sciences, Athens, GA 30602, [b]University of California, San Diego, The Skaggs School of Pharmacy and Pharmaceutical Sciences, 9500 Gilman Drive #0657, La Jolla, CA 92093-0657.[c]University of Washington, Department of Medicinal Chemistry, Seattle, WA 98195.[d]University of Washington, Department of Pharmaceutics, Seattle, WA 98195.

Results

Simulation of r_{app}, r_{avg} and R_P. To better understand the affect of time averaging on the r_{app}, r_{avg} and R_p, a simulation of a proton on phenyl molecule was performed. In the simulation, the phenyl approaches within 6 Å (r_{close}) of the heme iron. When the phenyl group flips with the orientation of the proton opposite to the heme, the maximum distance will be 5 Å greater or a total distance of 11 Å (r_{far}). In this simulation, the molecule can only be in two positions: close and far. The r_{app} in this case is:

$$r_{app} = \sqrt[6]{\frac{r_{close}^6 r_{far}^6}{f_{close} r_{far}^6 + f_{far} r_{close}^6}} \qquad \text{(Eq. 1a)}$$

$$r_{app} \cong \sqrt[6]{\frac{r_{close}^6}{f_{close}}} \qquad \text{(Eq. 1b)}$$

, where f_{close} and f_{far} are the fraction of time in the close and far positions, respectively. The apparent distance (r_{app}) is different than the time-averaged distance r_{avg}, when $f_{far} > 0$:

$$r_{avg} = f_{close} r_{close} + f_{far} r_{far} \qquad \text{(Eq. 2)}$$

Subsequently, R_P has similar time averaging behavior as r_{avg}, when $f_{far} > 0$:

$$R_P = f_{close} R_{close} + f_{far} R_{far} \qquad \text{(Eq. 3a)}$$

$$R_P \cong f_{close} R_{close} \qquad \text{(Eq. 3b)}$$

, where R_{close} and R_{far} are the close and far relaxation rates, respectively. For this simulation, the R_{close} was arbitrarly set to 2 sec^{-1}, which would make R_{far} based on distances equal to 0.053 sec^{-1} (i.e. $(11^{-6}/6^{-6})*2$).

Figure S1 shows the simulation of r_{app}, r_{avg} and R_P using the equations 1a, 2 and 3a. Figure S1A shows the effect of r_{app} and r_{avg}, when the molecule spends a certain fraction of the time close to the heme. When the molecule is oriented with the proton close 15% of the time (i.e. f_{close}=0.15), the r_{app} is 8 Å, while the r_{avg} is 10.25 Å. When the proton is in this oriented 50% of the time in the closer, the r_{app} is reduced to 6.7 Å

compared to an r_{avg} of 8.5 Å. When the simulated proton spends even a small amount of time at the closer distance, r_{app} skews to that distance. The skewing effect explains why distances measured using the Solomon-Bloombergen equation in a number of studies are not as dispersed as expected (e.g. *1*). In Figure S1B, the equation for R_P is plotted with respect to the fraction of time in the closer (f_{close}) orientation. The trend of R_P is linear with respect to f_{close} like r_{avg}, except that the slope is in the opposite direction, since the closer orientation is going to have a faster relaxation rate.

This linear relationship does not mean that it is possible to calculate r_{avg} from R_P without knowing the other parameters (e.g. r_{close}, r_{far}, f_{close} and f_{far}). It just means that the time averaging of known R_P rates and known distances are linear. Because of the r^6 distance relationship, R_P rate is considerably more sensitive to orientation than r_{app}. In cases were the molecule is highly mobile, the R_P rate may provide a better sense of the preferred orientation than r_{app}. On the other hand, if molecules are only in a single orientation (i.e. f_{far}=0), then r_{app} might also accurately represent the orientation because r_{app} would then equal r_{avg}. With that in mind, the relationship of R_P and r_{app} with respect to orientation must be treated carefully, but may be useful for qualitatively understanding the orientation and movement in the active site.

Size-Exclusion Chromatography Reveals the Aggregation State of Recombinant CYP3A4 in the Absence and Presence of Anapoe C12E10. To determine the aggregation state of CYP3A4 size-exclusion chromatography (SEC) was performed. Figure S2A shows the chromatogram of purified recombinant CYP3A4 in the absence of Anapoe C12E10. The retention time of the recombinant protein was 28.7 min. Analysis of the chromatogram in Figure S2B gave an average molecular weight of 236 kDa, which indicated that the recombinant CYP3A4 is primarily a tetramer (i.e. 236 kDa/60 kDa). Figure S2C shows the chromatogram of recombinant CYP3A4 in the presence of 2% Anapoe C10E12. The retention time was 32.5 min. and the molecular weight calculated from Figure S2D was 66 kDa, which indicated that the protein was a monomer.

CYP3A4 Absorbance Difference Spectra of Supersomes™ Overexpressing CYP3A4 in the Presence of MDZ and CBZ. Titrations of CYP3A4 were performed to determine, whether the affinity of MDZ to

purified CYP3A4 was similar to Supersomes™ overexpressing CYP3A4. The absorbance difference spectra of CYP3A4 in the presence of MDZ and CBZ in Supersomes™ are shown in Figure S3. The titration curves were fit using GEPASI and the equilibria shown in Scheme 2. The absorbance difference spectra of CYP3A4 in the presence of CBZ were too minute in Supersomes™ to make a reliable measurements (data not shown), so the $K_{D,CBZ}$ from purified CYP3A4 was used to fit the titration curves with GEPASI.

As with purified CYP3A4, type I absorbance differences were observed for CYP3A4 in the presence of MDZ in Supersomes™. The K_{D1} and K_{D2} determined by fitting the MDZ titration curves with GEPASI and equilibria in Scheme 2 were 6.7 ± 2.9 μM and 26.7 ± 5.8 μM, respectively. This was qualitatively similar to the K_D values that were determined in purified enzyme. However, the A_{max} was about 30% lower than purified CYP3A4 with a value of 0.0228 μM^{-1} cm^{-1} at 100 μM MDZ. The contrasting A_{max} and K_D*s* may reflect differences in the aggregation state and membrane interactions between membrane-bound CYP3A4 in Supersomes™ and purified *N*-terminal truncated CYP3A4.

Figures S3B and S3C show the effect of CBZ on the MDZ titration curves. As was observed in purified CYP3A4, Δε at 100 μM MDZ in the titration curves decreased with increasing the CBZ concentration. Fitting the titration curve in Figure S3C with GEPASI gave a $K_{D, CBZ}$' of 33.2 ± 2.0 μM, which is very close to the affinity of CBZ to purified enzyme.

Shifts and Broadening of MDZ and CBZ in the Presence of Oxidized and Reduced CYP3A4 Suggest that the Drugs are in Fast Exchange. Drugs bound to CYPs are continuously exchanged for drugs in bulk solvent. For experiments in this study, the ligand to protein ratio is relatively high. Therefore, the heme-induced R_P of drug protons is indirectly measured by probing drugs in bulk solvent. For this to be possible, drugs must exchange considerably faster than the relaxation rate of the protons, which is typically on the order of seconds.

Fast exchange of drug binding is usually determined by examining the temperature-dependence of the paramagnetically-induced T_1-relaxation (*1-5*). However, these experiments are complicated by two

factors. First, the spin state of P450s is temperature sensitive (*6-9*). Second, if the K_D is temperature-dependent, the drug may bind in a different orientations at different temperatures. To avoid these problems, fast exchange of P450-bound drugs was established by analyzing NMR peak shifts and broadening as previously described (*2, 10, 11*).

The CYP3A4-induced shifts and the broadening of MDZ and CBZ in Figure 5 show that these ligands are in fact in fast exchange with the protein. Further evidence of fast exchange is shown in Figure S4, which shows the effect of oxidized and reduced CYP3A4 on the NMR peaks of MDZ and CBZ. Figure S4A shows the broadening and shifting of the MDZ proton NMR peaks in the presence of CYP3A4. Because of a lower affinity, the shifts observed for CBZ are more modest than for MDZ (Figure S3). When both ligands are present in the same sample (Figure S4), the NMR spectra also shows distinct shifts and broadening. The shifts and broadening observed in Figures 5 and S4 conclusively show that the ligands are in fast exchange.

References

1. Regal, K. A., and Nelson, S. D. (2000) Orientation of caffeine within the active site of human cytochrome P450 1A2 based on NMR longitudinal (T_1) relaxation measurements, *Arch. Biochem. Biophys. 384*, 47-58.
2. Cameron, M. D., Wen, B., Allen, K. E., Roberts, A. G., Schuman, J. T., Campbell, A. P., Kunze, K. L., and Nelson, S. D. (2005) Cooperative binding of midazolam with testosterone and α-naphthoflavone within the CYP3A4 active site: a NMR T_1 paramagnetic relaxation study, *Biochemistry 44*, 14143-14151.
3. Cameron, M. D., Wen, B., Roberts, A. G., Atkins, W. M., Campbell, A. P., and Nelson, S. D. (2007) Cooperative binding of acetaminophen and caffeine within the P450 3A4 active site, *Chem. Res. Toxicol. 20*, 1434-1441.
4. Hummel, M. A., Gannett, P. M., Aguilar, J. S., and Tracy, T. S. (2004) Effector-mediated alteration of substrate orientation in cytochrome P450 2C9, *Biochemistry 43*, 7207-7214.
5. Modi, S., Primrose, W. U., Boyle, J. M., Gibson, C. F., Lian, L. Y., and Roberts, G. C. (1995) NMR studies of substrate binding to cytochrome P450 BM3: comparisons to cytochrome P450 cam, *Biochemistry 34*, 8982-8988.
6. Cinti, D. L., Sligar, S. G., Gibson, G. G., and Schenkman, J. B. (1979) Temperature-dependent spin equilibrium of microsomal and solubilized cytochrome P-450 from rat liver, *Biochemistry 18*, 36-42.
7. Fisher, M. T., and Sligar, S. G. (1987) Temperature jump relaxation kinetics of the $P\text{-}450_{cam}$ spin equilibrium, *Biochemistry 26*, 4797-4803.
8. Renaud, J. P., Davydov, D. R., Heirwegh, K. P., Mansuy, D., and Hui Bon Hoa, G. H. (1996) Thermodynamic studies of substrate binding and spin transitions in human cytochrome P-450 3A4 expressed in yeast microsomes, *Biochem. J. 319 (Pt 3)*, 675-681.

9. Ristau, O., Rein, H., Greschner, S., Janig, G. R., and Ruckpaul, K. (1979) Quantitative analysis of the spin equilibrium of cytochrome P-450 LM2 fraction from rabbit liver microsomes, *Acta Biol. Med. Ger. 38*, 177-185.

10. Gay, S. C., Shah, M. B., Talakad, J. C., Maekawa, K., Roberts, A. G., Wilderman, P. R., Sun, L., Yang, J. Y., Huelga, S. C., Hong, W. X., Zhang, Q., Stout, C. D., and Halpert, J. R. (2010) Crystal structure of a cytochrome P450 2B6 genetic variant in complex with the inhibitor 4-(4-chlorophenyl)imidazole at 2.0-Å resolution, *Mol. Pharmacol. 77*, 529-538.

11. Roberts, A. G., Sjogren, S. E., Fomina, N., Vu, K. T., Almutairi, A., and Halpert, J. R. (2011) NMR-derived models of amidopyrine and its metabolites in complexes with rabbit cytochrome P450 2B4 reveal a structural mechanism of sequential N-dealkylation, *Biochemistry 50*, 2123-2134.

12. Oda, A., Yamaotsu, N., and Hirono, S. (2005) New AMBER force field parameters of heme iron for cytochrome P450s determined by quantum chemical calculations of simplified models, *J. Comput. Chem. 26*, 818-826.

13. Yano, J. K., Wester, M. R., Schoch, G. A., Griffin, K. J., Stout, C. D., and Johnson, E. F. (2004) The structure of human microsomal cytochrome P450 3A4 determined by X-ray crystallography to 2.05 Å resolution, *J. Biol. Chem. 279*, 38091-38094.

14. Autenrieth, F., Tajkhorshid, E., Baudry, J., and Luthey-Schulten, Z. (2004) Classical force field parameters for the heme prosthetic group of cytochrome c, *J. Comput. Chem. 25*, 1613-1622.

Table S1. *Additional Force field parameters used for CYP3A4*[a]

Bond	Energy (kcal mol^{-1} $Å^{-2}$)	Distance (Å)[b]	Reference
Fe-S	87.589	2.377	(*12*)

Angle[c]	Energy (kcal $mol^{-1}rad^{-2}$)	Reference
Fe-S-C_b	21.646	(*12*)
N_P-Fe-S	13.277	(*12*)

Dihedral[c]	Energy (kcal mol^{-1})	Reference
C_b-S-Fe-N_P	0.034[d]	(*12*)

[a] Fe, heme iron; S, sulfur of C442; C_b, C_b of C442; N_P, pyrrole heme nitrogen.

[b] Equilibrium distance value from (*12*).

[c] The angles and dihedrals, used in the simulations, were calculated using the values measured from the CYP3A4 X-ray crystal structure (*13*).

[d] Autenrieth et al., 2004 obtained energy values for cytochrome c of 0.04 kcal mol^{-1} (*14*)

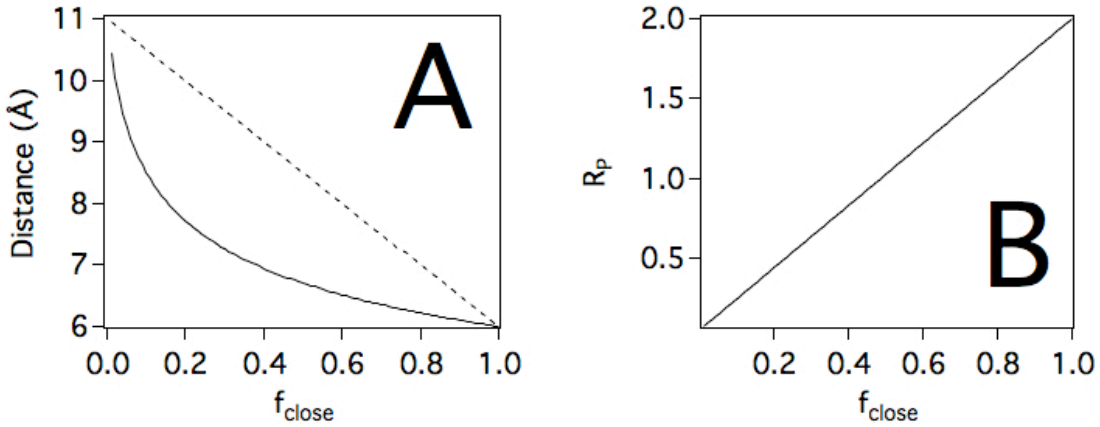

Figure S1. *The effect of time averaging on* r_{app}, r_{avg} *and* R_P. A) Calculated r_{app} and r_{avg} and B) Paramagnetic relaxation (R_P) with respect to the fraction of time in the closer orientation (i.e. f_{close}).

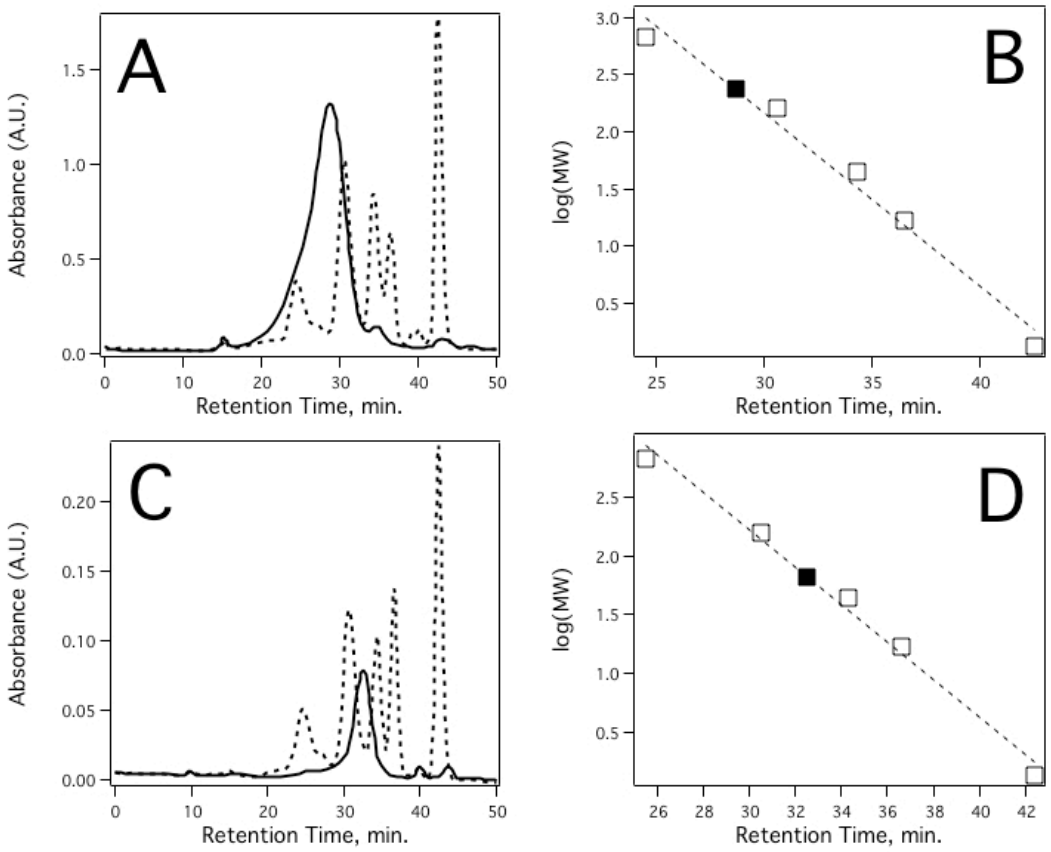

Figure S2. *Effect of 2% Anapoe C10E12 on the aggregation state of recombinant CYP3A4.* Size-exclusion chromatograms (left panels) and the analysis (right panels) of purified recombinant CYP3A4 (A-B) and purified recombinant CYP3A4 with 2% Anapoe C10E12 (C-D). The recombinant CYP3A4 and the standards in the size-exclusion chromatograms are shown as solid and dotted lines, respectively. The peak positions of the standards and the recombinant CYP3A4 are shown as open and closed squares, respectively. A line fit through the standard peak positions is shown as a dotted line. MW is the molecular weight in kDa.

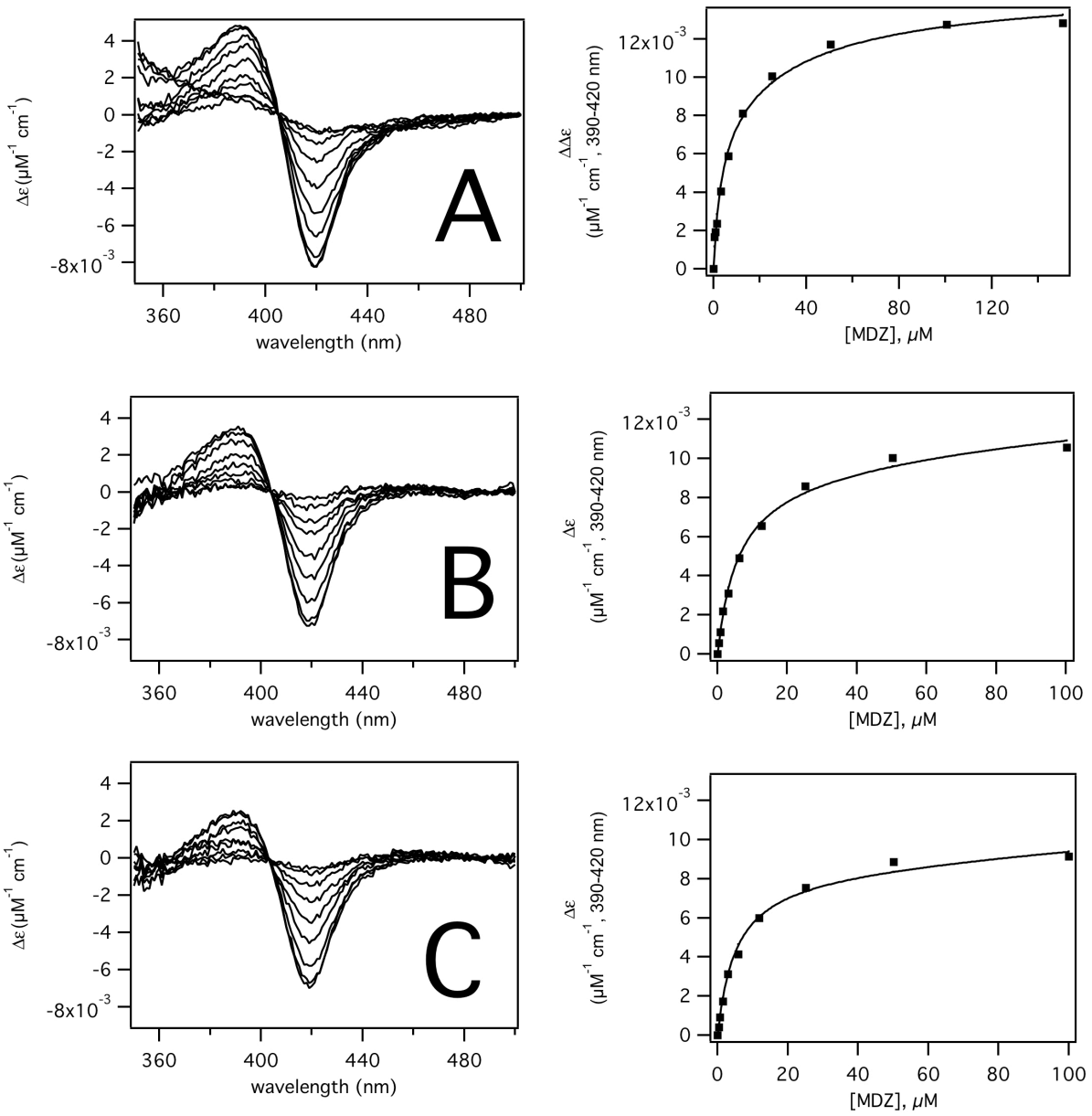

Figure S3. *Simple absorbance difference of CYP3A4 in Supersomes™ in the presence of midazolam (MDZ) and carbamazepine (CBZ).* The left and right panels show changes in the UV-visible of the CYP3A4 in the presence of A) MDZ, B) MDZ and 120 μM CBZ and C) MDZ and 240 μM CBZ. The panels on the left show the simple absorbance difference and the panels on the right show the amplitudes (solid squares) and fits. The curves in the right panels were simulated and fitted using GEPASI and the model that is shown in Scheme 2 with parameters from Table S2.

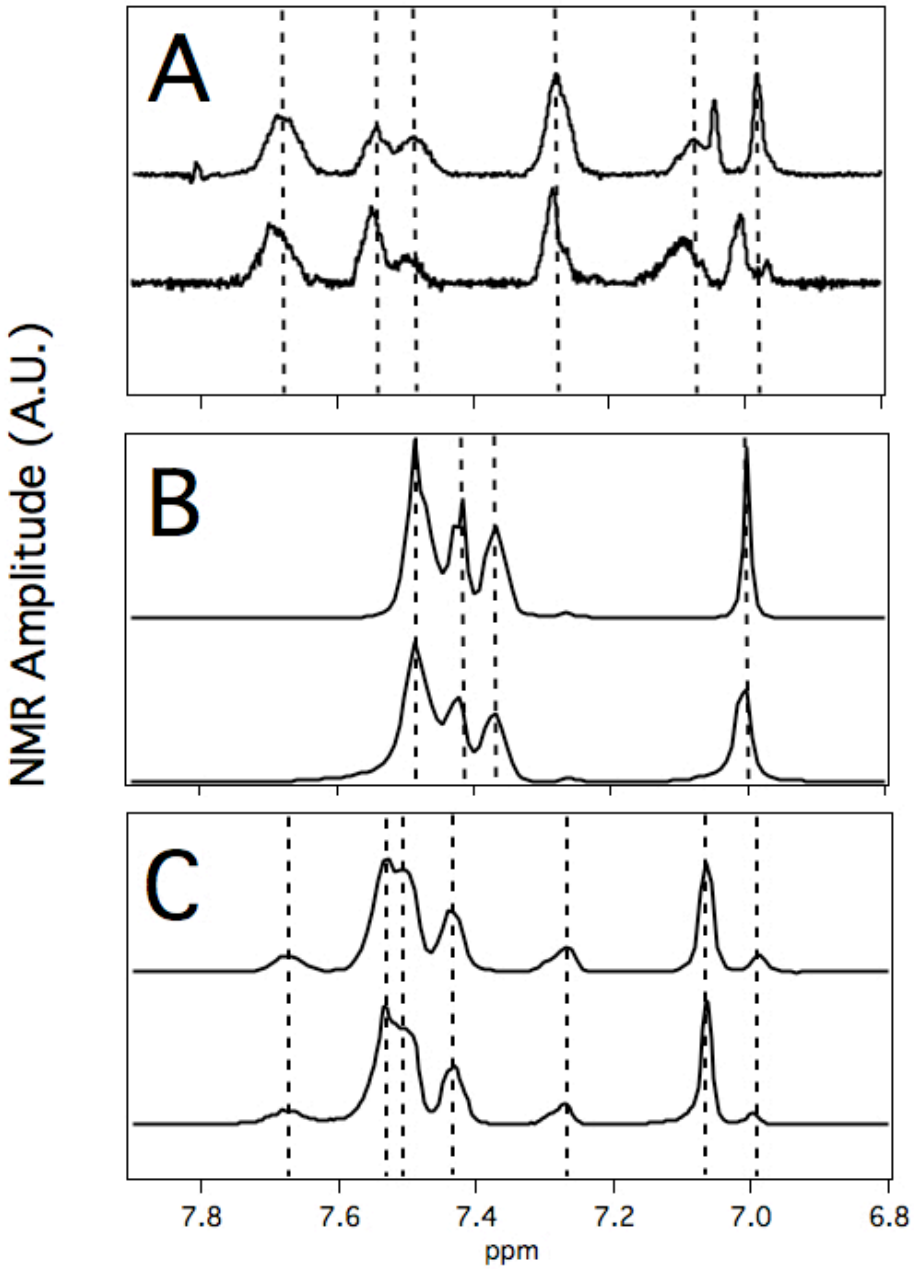

Figure S4. *Shifts and broadening of MDZ and CBZ proton NMR peaks in the presence of oxidized and reduced CYP3A4*. NMR spectra in the aromatic region between 6-8 ppm of A) 260 μM MDZ, B) 260 μM CBZ and C) 260 μM MDZ and CBZ in the presence of oxidized (top) and reduced (bottom) CYP3A4.